Chondrobags: A high throughput alginate-fibronectin micromass platform for *in vitro* human cartilage formation

Kimia Witte [1,3], María C. de Andrés [2,4], Julia Wells [2], Matthew J. Dalby [1], Manuel Salmeron-Sanchez *[1] and Richard O. C. Oreffo *[2]

[1] Centre for the Cellular Microenvironment, University of Glasgow, Glasgow, UK
[2] Centre for Human Development, Stem Cells and Regeneration, Institute of Developmental Sciences, Faculty of Medicine, University of Southampton, Southampton, UK
[3] Strathclyde Institute of Pharmacy and Biomedical Sciences, University of Strathclyde, Glasgow, UK
[4] INIBIC-Complexo Hospitalario Universitario A Coruña (CHUAC), Rheumatology Division, A Coruña, Spain

E-mail: kimia.witte@strath.ac.uk, MA.Carmen.De.Andres.Gonzalez@sergas.es, j.a.wells@soton.ac.uk, matthew.dalby@glasgow.ac.uk, manuel.salmeron-sanchez@glasgow.ac.uk and richard.oreffo@soton.ac.uk

Received xxxxxx
Accepted for publication xxxxxx
Published xxxxxx

Abstract

The maintenance and expansion of the cells required for formation of tissue-engineered cartilage has, to date, proven difficult. This is, in part, due to the initial solid phase extracellular matrix demanded by the cells inhabiting this avascular tissue. Herein, we engineer an innovative alginate-fibronectin microfluidic-based carrier construct (termed a chondrobag) equipped with solid phase presentation of growth factors that support skeletal stem cell chondrogenic differentiation while preserving human articular chondrocyte phenotype. Results demonstrate biocompatibility, cell viability, proliferation and tissue-specific differentiation for chondrogenic markers *SOX9*, *COL2A1* and *ACAN*. Modulation of chondrogenic cell hypertrophy, following culture within chondrobags loaded with TGF-β1, was confirmed by down-regulation of hypertrophic genes *COL10A1* and *MMP13*. MicroRNAs involved in the chondrogenesis process, including miR-140, miR-146b and miR-138 were observed. Results demonstrate the generation of a novel high-throughput, microfluidic-based, scalable carrier that supports human chondrogenesis with significant implications therein for cartilage repair-based therapies.

Keywords: biofabrication, droplet-based microfluidics, stem cells, chondrogenesis, hydrogels, fibronectin

1. Introduction

Cartilage lesions represent an important technical challenge for tissue engineering given the avascular nature of this tissue, which often leads to defective intrinsic healing.[1] Unattended cartilage damage can result in osteoarthritis (OA), the most prevalent chronic pathology of joints.[1, 2] Defective articular cartilage and alterations made to the state of bone at joint margins for instance, are among a diverse set of signs and symptoms associated with OA.[3] Chondrocytes, derived from the native tissue, have been examined as an apparent cell source of the formation of neocartilage.

Over the last decades, interest in stem cells for tissue engineering applications has noticeably increased, given their capacity for self-renewal and multi-lineage differentiation.[4] Chondrocytes or chondroprogenitors, derived from stromal progenitors, need to be guided in the formation of native hyaline cartilage, to avert dedifferentiation and, critically, to ensure the generation of pre-eminent tissue reconstruction *in vivo* that resembles the complex cellular and extracellular matrix (ECM) make-up in the native tissue. In addition, the generated tissue must be permissive to typical load-bearing while providing long-lasting joint performance.[5] A wealth of literature suggests micromass or pellet culture models, offer an appropriate method for generating small-scale micron sized tissues of engineered neocartilage *in vitro*. Furthermore, more advanced cartilage-like tissues exhibiting improved mechanical properties have been made exploiting 3D models for cell proliferation and differentiation.[6] These systems facilitate interactions between the cell and the requisite cellular environment/matrix.[7] However, these 3D systems still display an overall lack of homogeneity in cell responses related to the necrotic cores,[8] that could be assigned to a list of contributing factors including: (i) the non-physiological closely compacted cells that are formed during initial stages of culture, (ii) the existence of necrotic cores enclosed by *in vitro*/*ex vivo* cell clusters as a consequence of high cell number, (iii) sub-standard physiological culture conditions and, (iv) diffusion limitations by uncontrolled establishment of chemical gradients throughout samples.[9]

Recent studies have explored high throughput strategies for micro-tissue modeling.[10, 11] Thus, microfluidics offers significant potential for the generation of high-throughput cell culture prototypes, presenting unparalleled spatio-temporal control on the requisite micro-environmental conditions.[12, 13] To this objective, we present an experimental droplet-based microfluidic device for the fabrication and the culture of 3D micromass constructs of mature chondrocytes and skeletal stem cells (SSCs) generated under constant laminar flow, termed 'chondrobags'. Chondrobags are highly mono-dispersed, pearl-lace interlinking hydrogel-based structures with pearl and lace subunit sizes ranging from 100 and 150 μm. We note that SSCs are a bone marrow derived multipotent mesenchymal stromal cell (MSCs) population with the established propensity for skeletal regeneration.[14]

It is clear that materials used for cartilage tissue engineering significantly affect the pattern of the gene expression of the chondrocyte population therein.[15] Mimicking the hydrated environment of native cartilage, hydrogels offer an attractive approach for the development of cartilage regenerative strategies. Hydrogels are made by crosslinking naturally derived polymers, such as collagen and alginate, as well as polymers manufactured, such as polyethylene glycol and polyacrylamide. These polymer networks are crosslinked hydrophilic systems that are able to retain high volumes of fluid without dissolving. This allows construction of a microenvironment for cells, which takes on the appearance of native tissue through facilitation of waste and nutrients exchange.[16] Furthermore, hydrogels offer a strategy for the homogeneous encapsulation of cells of interest in comparison to numerous reported scaffolds. Critically, the mechanical properties of hydrogels, such as viscoelasticity, typically, can be fine-tuned to mimic those found in the native cartilage.[17] Alginate is a biocompatible material that is used to form microporous hydrogels.[18] The permeable nature of the alginate hydrogel allows diffusion of nutrients, molecules and facilitates communication and contact between cells, providing a rich ECM-like environment that can support cell viability.[19] Indeed, a number of studies have shown that MSCs-laden alginate hydrogels can support chondrogenesis.[19-21]

Naturally found alginate polymers offer good hydrophilicity and allow ionic crosslinking. However, alginate hydrogels lack intrinsic cell adhesion domains, which diminish their biological activity and subsequently hamper their use in tissue engineering.[22] Approaches to overcome this limitation have centred on the incorporation of molecules such as Arg-Gly-Asp (RGD)-based peptides to facilitate integrin binding.[16] The display of an RGD sequence in alginate hydrogels provides a strategy for control over the phenotype of participating chondrocytes, osteoblasts, and MSCs.[23] The functional RGD peptide is a cell adhesion motif, found in ECM proteins including fibronectin (FN)[24] and suggested to positively contribute to the chondrogenesis of MSCs, although, the effect is controversial and dependent on application.[25] FN has been denoted to initiate the cellular signalling of chondrocyte differentiation[26] and is critical in orchestration of the assembly of further ECM proteins including collagen.[27] Furthermore, the down-regulation of FN can alter cell morphology and shape resulting in reduced chondrogenic differentiation.[28]

Cationic molecules such as transforming growth factor beta (TGF-β) display affinity towards the negatively charged alginate molecules by way of the Coulombic interaction and can be freed from alginate with slow kinetics.[29] In addition, the 12th–14th type III repeats of fibronectin (FN III12–14) bind to the TGF-β superfamily with high affinity.[30] The TGF-β superfamily is made up of three type of isoforms (TGF-β1, TGF-β2, and TGF-β3); however, exclusively, TGF-β1 and TGF-β3 are relevant for stem cell chondrogenic differentiation.[31, 32] TGF-β3 displays a higher chondrogenic promise as compared to TGF-β1, leading to enhanced differentiation.[33] However, it remains unclear, if this TGF-β3 enhanced differentiation is correlated with higher responsiveness for chondrocyte hypertrophy.

We have generated an innovative alginate-FN micron-sized subunit carrier for chondrogenesis – *chondrobags*. This novel system allows high-throughput fabrication of reproducible microgels with precise control over the density of embedded cells, shape and mono-dispersity. The chondrobags incorporate FN to immobilise growth factors and encapsulated cells while bypassing the diffusion limit for oxygen and nutrition given the chondrobag size. In addition, using pearl-lace interlinking hydrogel-based structures, chondrobags can be used for alternative microfluidic-based bioprinting.[34] The alginate-FN chondrobags presenting TGF-β1 in solid phase provide a favourable chondrogenic microenvironment for specific differentiation of *in situ* cultured skeletal stem cells

(SSCs) and human articular chondrocytes (HACs), with implications therein for future tissue engineering applications.

2. Materials and Methods

2.1 Human bone marrow derived SSCs isolation and culture

Bone marrow was sourced from a patient undertaking total hip replacement surgery at Spire Hospital in conjunction with the full ethical consent and approval from the hospital ethics committee (LREC 194/99/w, 27/10/10), through which informed patient consent was attained. All procedures making use of human tissue and cells were carried out in agreement with stipulated recommendations and regulations. Bone marrow (male 70 years of age) was acquired and used for isolating and culturing human bone marrow derived SSCs as previously detailed.[35] Washed bone marrow mixture was sieved through a 70 μm cell filter and separated using Lymphoprep™ (Lonza). Prior to a wash step with magnetic activated cell sorting (MACS) buffer (BSA and EDTA in PBS), harvested mononuclear cells were incubated in blocking buffer (α-MEM, 10% human serum, 5% fetal calf serum (FCS) and 10 mg/mL bovine serum albumin). Cells were incubated in 1 mL of hybridoma-based STRO-1 antibody and following a wash with MACS buffer were re-suspended in 1 mL containing 800 μL MACs buffer and 200 μL rat anti-mouse IgM microbeads (Miltenyi Biotec Ltd). A second MACS harvest for target cells was followed by washing with MACS buffer. Isolated target cells were washed and re-suspended in α-MEM containing 10% FCS and 1% penicillin/streptomycin (P/S) and cultured in tissue culture flasks.

2.2 Human articular chondrocytes isolation and culture

Femoral head was acquired from a male patient (61 years of age) undergoing total hip replacement surgery at Southampton General Hospital, in conjunction with the full ethical consent and approval from the hospital ethics committee (LREC 194/99/w, 27/10/10), with informed patient consent attained. The OA femoral head was classified as end stage OA (3–5 OARSI). The articular cartilage was dissected from the femoral head and sliced into small sections within 6 hours post-surgery. Cartilage sections were incubated for 30 minutes at 37 °C in 10% trypsin (Sigma Aldrich) followed by 15 minutes in 0.1% hyaluronidase (Sigma Aldrich) following a wash with PBS. This trypsin-hyaluronidase step was followed by a further wash and incubation for 12–15 hours at 37°C in 1% collagenase B (Roche Diagnostics). The suspension containing the digested articular chondrocytes was filtered through a 70 μm filter. Isolated chondrocytes were re-suspended in DMEM/F12 containing 5% FCS, 1% insulin-transferrin-selenium (ITS) (Sigma-Aldrich), 1% P/S and 0.2% of ascorbic acid (Sigma-Aldrich), and placed into tissue culture flasks.

2.3 Microfluidic fabrication

Co-flow focusing glass capillary device (Figure 1 A and B) for pearl-lace like microgel production developed in this study, was first reported by Witte et al.[34] Glass capillaries (< 1.8 mm, TST150-6 and TW100-6, World precision instruments, Inc.) were tapered to desired hole sizes (0.04 - 0.07 mm) using a micropipette puller (P-97, Sutter Instruments) and centrally aligned in a square capillary of 2 mm ID (World precision instruments, Inc.). Sigmacote (Sigma-Aldrich) was used to modify the glass surface generating a hydrophobic layer. Capillaries were fixed on a cover-slide and using soft tubing, coupled with controllable syringe pumps (Harvard Apparatus).

2.3 Cell encapsulation

Both SSCs and HACs populations were initially treated for 40 min with collagenase IV (200 μg/mL) in α-MEM prior to detachment from culture plates using 0.025% (w/v) Trypsin–EDTA with 0.05% glucose for 10 min at 37°C. To prepare a 2% alginate mixture, both cell types were individually re-suspended in the corresponding basal media and subsequently mixed 1:1 together with a medium viscosity 4% (w/v) sodium alginate (Sigma-Aldrich, UK) solution. FN sourced from human plasma (Sigma) was added to the mixture to give a final concentration 20 μg/mL. The water-based alginic cell mixture entered the microfluidic device through one of the two channels of a theta-shaped capillary, while leaving the other channel for 200 mM calcium chloride aqueous solution. Mineral oil (Sigma-Aldrich, UK) with 2% Span 80 (Sigma-Aldrich, UK) was introduced as the continuous phase through a square-shaped housing capillary for dispersing the two water-based solutions as they mixed within the flow focusing regime. Pre-warmed basal culture media was used as the collection solution for formed hydrogels. This step was followed by a 100 mM calcium chloride wash before culturing in either basal media or chondrogenic media comprising 10 nM dexamethasone, 100 μM ascorbic acid, 10 μg/mL ITS and 10 ng/mL of either TGF-β1 or TGF-β3 (Peprotech) at 37°C and 5% CO_2 in a humidified atmosphere. Media (chondrogenic differentiation media and basal media) was changed every two days until the end of the experiment at day 28.

2.4 Viability assay

Viability studies were carried out following incubation of the cell-laden hydrogels for an hour at 37°C in a 100 mM calcium chloride solution containing 2 μM calcein and 2 μM ethidium homodimer-1 (EthD-1) (Viability/Cytotoxicity Kit, Life Technologies, UK). For the viability calculation, the total number of live cells (stained green) were analysed in comparison to the total number of cells (stained either green or red). Viability was expressed as a percentage of the control. The hardware and software from EVOS Fl Colour Cell Imaging System were used for assigning the stained samples (green for live and red for dead cells). For measuring the pixel intensity of the fluorescence signals, sample images were processed using ImageJ software

version 1.51 (100) and later graphed using GraphPad Prism (version 8.0 software).

2.5 RNA isolation and quantification

Chondrobags were prepared with a PBS wash at the end of the culturing period, prior to a 10 minutes incubation at 37°C incubation with 1 mL of dissolving buffer (0.055M sodium citrate, in 0.03M EDTA, 0.15M NaCl, pH 6.8) at 1,000 rpm. This step was followed by centrifugation at 10,000 rpm for two minutes, a PBS wash and another round of centrifugation at 14,500 rpm for two minutes. 350 mL of RLT Plus Buffer was used to lyse the pellets formed by the cells. The lysed cell mixture was added to 540 mL RNA-free water and 10 mL Protease K solution (Qiagen) and further incubated for 10 minutes at 1000 rpm, 55°C. AllPrep DNA/RNA/miRNA Universal Kit (Qiagen) was used to isolate RNA from the samples following the guidelines by the manufacturer. Extracted RNA samples were quantified using a Nanodrop ND-1000 spectrophotometer.

2.6 cDNA synthesis and mRNA expression analysis

cDNA synthesis and real time quantitative PCR (qPCR) were carried out to analyse expression of mRNA in human SSCs and HACs. SuperScript® VILO cDNA Synthesis kit from Applied Biosystems was used for the synthesis of cDNA from sample containing isolated RNA. In brief, RNA was mixed with 2 µL 5X VILO™ reaction mix and 1 µL 10X SuperScript® enzyme. The mixture was subsequently incubated for 10 minutes at 25°C and, thereafter, by a further incubation at 42°C for 2 hours and 85°C for 5 minutes. qPCR was carried out with 10 µL of GoTaq master mix (Promega), 5 µL of upH_2O and 2 µL of reverse primer and 2 µL of forward primer for the gene of interest (primers listed in Table S1) and 1 µL of sample containing isolated RNA. A 96 well-plate with each well containing a final mixture of 20 µL was later analysed using Applied Biosystems, 7500 Real Time PCR system. Acquired data was analysed using version 2.0.5 program of Applied Biosystems 7500 System SDS. To identify the most stable housekeeping genes, standard optimisation procedures were performed. For normalising Ct (cross-over threshold) values for SSCs experiments, *ACTB* as the endogenous housekeeping gene and for HACs analysis, *GAPDH* were used respectively. The fold expression levels were calculated using delta-delta Ct method for each target gene. All the sample readouts as well as control (negative control with no cDNA) were analysed from triplicates.

2.7 miRNA expression analysis

RNA extracted as detailed in *RNA isolation and quantification* were assessed for expression of: miR-140, miR-146b or miR-138 using TaqMan® MiRNA Assays (Table S2). Every individual assay contained two primers: one primer was used for cDNA synthesis and the second primer was used to perform TaqMan q-PCR. For generating cDNA specific to each individual assay, specific miRNA from total RNA was generated with TaqMan® MiRNA Reverse Transcription Kit using a modified protocol from the manufacturer. In brief, a reaction mixture containing of 3.58 µL upH_2O, 0.75 µL 10X Buffer, 1.88 µL of RNase inhibitor, 1.50 µL of RT primer, 0.08 µL of dNTPs and 10 ng of total RNA was made and incubated at 16°C for 30 minutes followed by 30 minutes at 42°C and further 5 minutes of incubation at 85°C before termination at 42°C. qPCR was carried out with 5 µL of TaqMan® Universal PCR Master Mix containing No AmpErase® UNG from Life technologies. The qPCR also included 3.34 µL of upH_2O, 0.5 µL of TM primer and 0.8 µL of cDNA. A 96 well-plate containing this mixture was assessed using Applied Biosystems, 7500 Real Time PCR system and data gathered analysed using version 2.0.5 program from Applied Biosystems 7500 System SDS. Standard optimisation procedures were performed to determine the appropriate housekeeping gene for the study of miRNA expression. For normalising Ct values, RNU44, was used as a housekeeping control RNA for miRNA. To calculate the fold expression level of each gene of interest, delta-delta Ct method was employed. All sample readouts, including negative controls (no cDNA), were analysed from duplicates.

2.8 Enzyme Linked Immunosorbent Assay (ELISA)

Solid Phase Sandwich ELISA for transforming Growth Factor Beta 1 and 3 release from the alginate construct were measured using Human TGF-β1 DuoSet ELISA (DY240-05) and Human TGF-β3 DuoSet ELISA (DY243) kits from R&D systems. 0.5 mL of alginate micro-beads (with and without FN at 20 µg/mL concentration) were soaked in 5 mL DMEM media containing either TGF-β1 or TGF-β3 at the concentration of 10 ng/mL overnight. The following day, micro-beads were placed into fresh media and samples for ELISA were taken at 1.5, 3, 6 and 24 hours. ELISA steps were carried out according to manufacturer's instructions and the readouts performed using BioTek™ Synergy™ HT Multi-Detection Microplate Reader.

2.9 Histology

Chondrobags were washed in 0.1 mM calcium chloride and fixed in 10% buffered formalin (neutral) prior to histological analysis. Specimens were dried using a series of graded ethanols, embedded in OCT (CellPath, UK) and cryo-sectioned at 5 µm thickness. Dehydrated sections were collected onto APEs coated slides, air dried for 30 min and stored at -20°C until required for staining. For histological evaluation, sections were warmed at 37°C for 30 min and washed in RO water prior to staining with Alcian Blue/Sirius Red and Safranin O/Fast Green. Briefly, sections were stained with Weigert's haematoxylin (A and B, 1:1 mix, Clin-Tech, UK) for 10 min prior to staining with 0.5% Alcian Blue (Sigma, UK) for 10 min, followed with molybdophosphoric acid (Sigma, UK) for 10 min and finally with Sirius Red (Clin-Tech, UK) for an hour or were stained with Fast Green (FCF) solution for 5 minutes followed with Safranin O for 5 minutes. Between each staining step, slides were rinsed in a water bath for 1 min and drained. Slides were finally dehydrated through increasing ethanol concentrations and cleared in Histoclear (50%, 90%, 100%-1, 100%-2 ethanol and Histoclear-1 and 2

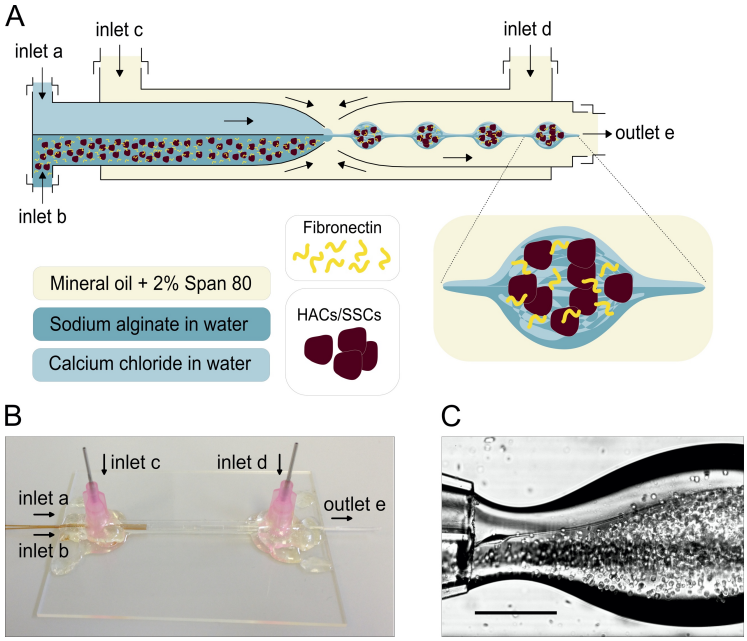

Figure 1. Droplet-based microfluidic setup, mono-dispersity and encapsulation. (A) Schematic representation of the microfluidic device and encapsulation of eukaryotic cells. (B) Image of the capillary based microfluidic device. (C) A snapshot of encapsulation of cells using the microfluidic device. Scale bar: 100 µm. HACs: human articular chondrocytes, SSCs: Stro-1 enriched skeletal stem cells.

each for 30 seconds) before being mounted in p-xylene bis-pyridinium bromide (DPX). Sections were observed using an Olympus dotSlide Virtual Microscopy System and images processed using Olympus OlyVIA 2.9 image analysis software.

2.10 Statistical Analysis

Data are presented as mean values and standard deviations (SD). Statistical analysis was performed by a one-way ANOVA, a Tukey post-hoc test and Student's *t* test in GraphPad Prism™ 8 software with a level of significance of $p < 0.1$ marked by *, $p < 0.05$ marked by **, $p < 0.001$ marked by *** and $p < 0.0001$ marked by ****.

3. Results and Discussion

3.1 Microfluidic fabrication of mono-dispersed alginate-fibronectin chondrobags and encapsulation of SSCs and HACs

SSCs and HACs were encapsulated in pearl-lace like chondrobags using co-flow focusing glass capillary devices (Figure 1A–C and Supplementary Video 1 and 2). The design was optimised in respect to our previous report for encapsulation of a co-culture of MSCs and engineered bacteria.[34]

The alginate-calcium composite is a diffusion-based hydrogel prepared by ionic cross-linking. Diffusion is a time-dependent process and for this reason, fully homogeneous hydrogels can never be fully attained. Nevertheless, as the bead size is reduced, heterogeneity is reduced between formed hydrogels. As a consequence, Calcium diffusion occurred rapidly in the micro-sized beads leading to improved and high encapsulation efficiency (> 99%) (Figure 2A) within each microgel (Supplementary Video 2), leading to the generation of reproducible chondrobags (Figure 2B). The shape and size of the pearl-lace microgel construct chosen for this study provided efficient volume ratios between material and cell, eliminating the diffusion cap of 100 to 200 µm for the transport of oxygen, nutrients including ingress of vital biomolecules for encapsulated cells and facilitation of removal of cell waste.[36] Chondrobags were generated at 5-10 units per second within selected flow rates containing ~ 2.6e+07 cells/mL (Figure 2C and Figure 2D). This resulted in cells residing in close proximity (~ 10^3 cells per chondrobag, Figure 2E) while facilitating nutrition and waste diffusing through the porous micro-structures of the alginate-FN hydrogel (Figure 2F).

The superiority of 3D over 2D cultures to enhance stem cells functions are well documented, and the culture of SSCs in 3D has previously demonstrated enhanced stromal differentiation along the chondrogenic lineage.[37] In contrast to 2D cultures, the culture of stem cells in 3D promoted enhanced cell-cell contact; facilitating exposure of cells to substrates with different physical properties including viscoelasticity and topography together with the display of assorted endogenous and exogenous ECM adhesion motifs for integrins.[37] The application of droplet microfluidics for 3D micromass formation with HACs and SSCs, together with *in situ* fine temporal control over the constituents of biomaterials provided a powerful platform to deliver reproducible and, crucially, a high-throughput formation of functional micromass constructs.[38, 39] Such a strategy has been undertaken using pluripotent stem cells.[40-42] The incorporation of mechanical stress[43] and hypoxia, [44] offer

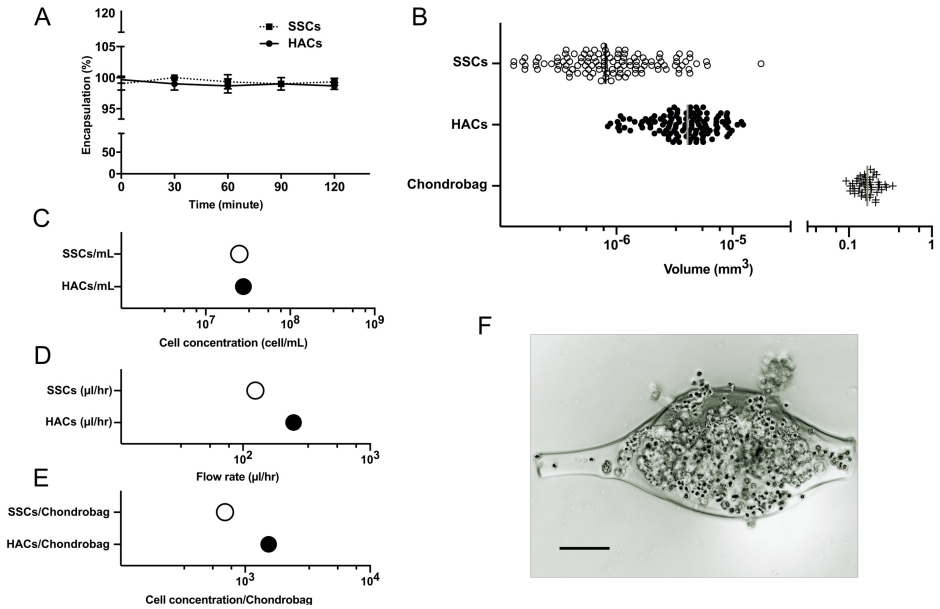

Figure 2. Encapsulation efficiency, cell density and volume mono-dispersity of chondrobags. (A) Cell (HACs and SSCs) encapsulation efficiency. The cell counts at each time point are the result of 8 measurements sequentially acquired at 30-min intervals at room temperature for 2 h. (B) Volume distribution of produced chondrobags of two miscible fluid streams under laminar flow conditions using flow rates of 125 - 250 µL h^{-1} for the two inner phases and 3000 µL h^{-1} for the outer phase. The median volume of the formed chondrobag was 0.16 mm^3 with a RSD of 3.2%. (C) Cell concentrations used in this study. (D) Selected flow rates. (E) Cell concentration per chondrobag. (F) A snapshot of chondrobag filled with HAC. Scale bar: 100 µm. HACs: human articular chondrocytes, SSCs: Stro-1 enriched skeletal stem cells.

future approaches to enhance and further mimic the physiological environment to enhance chondrogenic differentiation.

It has been shown that a bone-like physicochemical microenvironment can override chondroinductive signals including TGF-β1. The extracellular calcium-sensing receptor (CaSR) of human BM-derived MSCs has shown to become hyperstimulated by bone-like biomimetic hydroxyapatite (BBHAp).[45] However, in this study, the calcium concentration used to gel the alginic acid was retained at the same level for all samples including the negative control constructs while studying the impact of TGF-β1 and TGF-β3 separately in FN containing chondrobags.

Studies have established that the permeable structure of a scaffold can aid cell attachment, proliferation and differentiation, which can lead to generation of the phenotype of interest in a cell.[32, 46] Chondrobags combine alginate and FN to provide a cost-effective facile strategy for three-dimensional construct generation (18 - 36k chondrobags per hour) with a clear potential for cartilage tissue engineering. Correct porosity provides appropriate shape and environmental cues through mimicry of the chondrocyte lacunae to facilitate proliferation and differentiation. The favorable porosity, thin walls and excellent interconnectivity between pores of the hydrogel, contribute to nutrient and metabolic waste exchange. The induced condensation of HACS and SSCs in chondrobags is a significant milestone in comparison to current conventional scaffold-free systems requiring 3D culture, predominantly based on micromass pellets derived using centrifugation.[8] The use of centrifugation, as an initial step, typically generates restrictive cell to cell and cell to ECM interactions, resulting in high variability in the time required to form 3D aggregates.[9] In addition, traditional macro-pellet models are often too large and, typically, suffer from heterogeneity of cell phenotype and the formation of necrotic cores.[8, 47] As shown in Supplementary Video 3, pearl-on-thread chondrobags can be used as a low-cost cell-laden bioprinting alternative.

3.2 Skeletal cell viability, cell cluster and micro-mass formation in chondrobags

The advantages of reduced shear stress experienced during cell encapsulation in chondrobags due to the channel design and low flow rates of this microfluidic design,[34] contributed to high cell viability observed throughout the hydrogel. Evaluation of the cell viability of HACs and SSCs demonstrated the presence of live cells (>90%) with negligible necrotic cells present in the central regions of cell clusters in the chondrobags. Viability and biocompatibility of alginate-FN chondrobags was confirmed 1, 3 and 24 hours following encapsulation and, crucially, at the conclusion of the studies, on day 28. Figure 3A-D demonstrate the level of viability observed following encapsulation at day 0 and at 28 days. For HACs, no differences in cell viability were observed between cells cultured in chondrogenic media with TGF-β1 or TGF-β3 (Figure 3A-B). Enhanced HACs cell numbers were observed within chondrobags loaded with TGF-β3 with an average of 11.8 cells per cluster, as compared to 8.3 cells per cluster in TGF-β1 and 1.8 cells per cluster for control samples (Figure 3H). This variation is likely a consequence of differences in cell proliferation, given all the samples comprised the same initial cell density per chondrobag (Figure 2E). In addition to higher cell counts per cluster (1.4 times), the area of clusters in TGF-β3 was almost twice (1.9 times, normalised against

area of cell clusters in control sample) the size as compared to those stimulated with TGF-β1 (Figure 3G). Interestingly, this finding is consistent with the cell volume expansion of hypertrophic chondrocytes in the growth plate, as a consequence of an increase in organelles and increased metabolic activity.[48] Mueller and collaborators have reported this to be the case for the enhancement of hypertrophy in MSC chondrogenesis.[49]

SSCs encapsulated within chondrobags displayed a discrete increase in the numbers of necrotic cells following stimulation with TGF-β3 and TGF-β1, as compared to the control samples (Figure 3C-D). The micromass samples generated by SSCs within chondrobags, stimulated with TGF-β1 or TGF-β3, were noted to be more compact with no clear border (space) between cells within the same cluster/colony (Figure 3C and

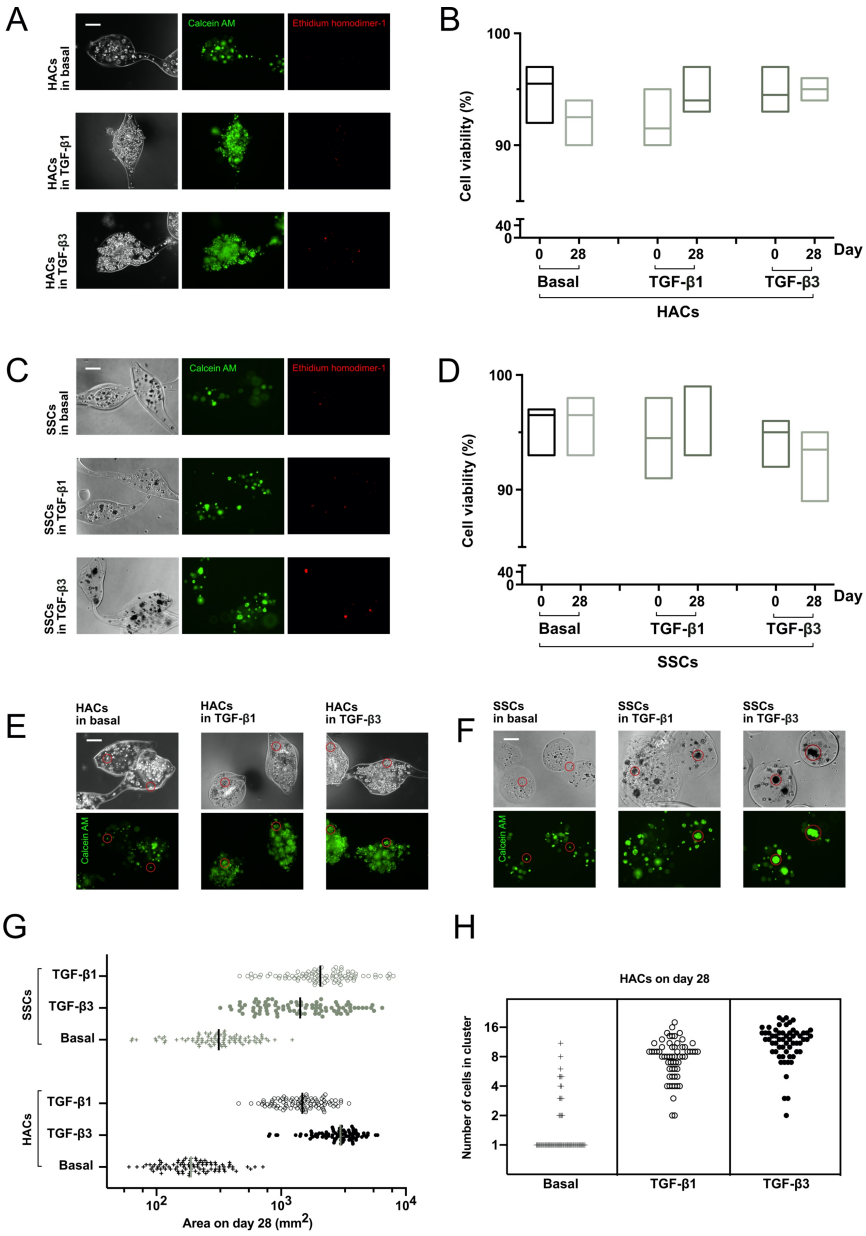

Figure 3. Skeletal cell viability, cell cluster and micro-mass formation in chondrobags. (A) Microscopy images of alginate-fibronectin (FN) chondrobags containing human articular chondrocytes (HACs) cultured in the presence of TGF-β1 or TGF-β3 for up to 28 days relative to untreated control. (B) HACs viability graph. (C) Microscopy images of alginate-FN chondrobags containing Stro-1 enriched skeletal stem cells (SSCs) cultured in the presence of TGF-β1 or TGF-β3 for up to 28 days relative to untreated control. (D) SSCs viability graph. (E) Microscopy images of alginate-FN chondrobags containing HACs cultured in the presence of TGF-β1 or TGF-β3 for up to 28 days relative to untreated basal control. Individual cells are highlighted within a red circle. (F) Microscopy images of alginate-FN chondrobags containing SSCs cultured in the presence of TGF-β1 or TGF-β3 for up to 28 days relative to untreated basal control. Micro-masses are highlighted within a red circle. (G) Graph with area of SSCs and HACs cultured in the presence of TGF-β1 or TGF-β3 for up to 28 days relative to untreated basal control. (H) Graph with number of cells found in clusters containing HACs after 28 days. Cells in green are stained with Calcein AM. Scale bar: 100 μm. The hydrogel was stained with Viability/Cytotoxicity Kit with viable cells in green (Calcein AM) and non-viable cells in red (Ethidium homodimer-1). Scale bar: 100 μm. N ≥ 5 – 10 microgels were analysed for each condition. Additional images can be found in Supplementary Figure 1.

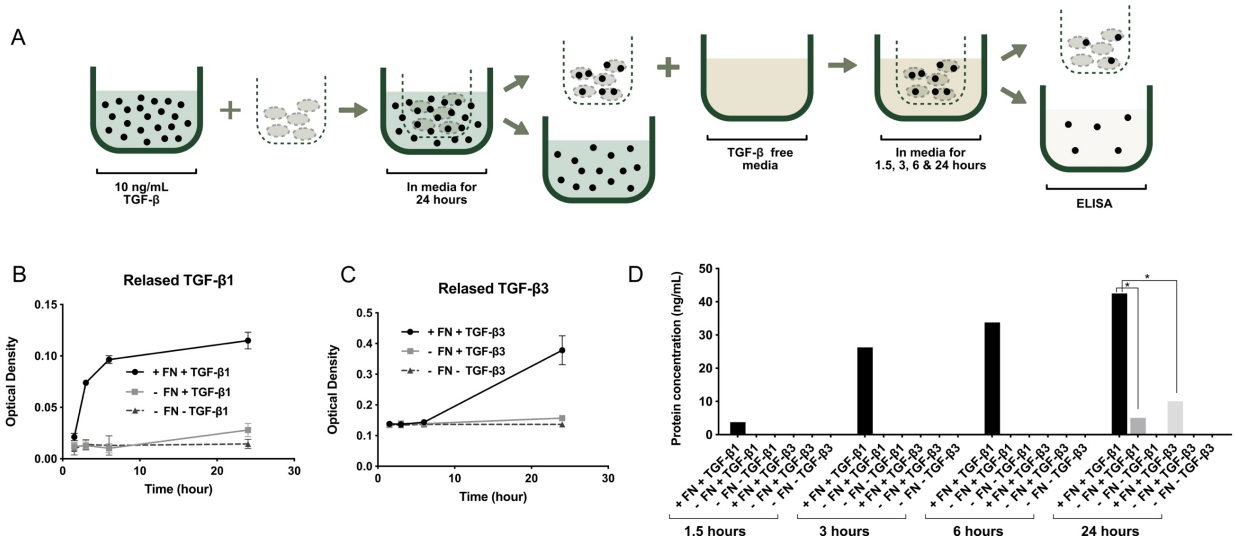

Figure 4. TGF-β binding affinity for the full-length fibronectin (FN) in chondrobags. Infographic detailing the ELISA sample preparation. The following samples were collected at 1.5, 3, 6 and 24 hours; fibronectin-alginate with and without TGF-β1, FN-alginate with and without TGF-β3, alginate only with and without TGF-β1 as control, alginate only with and without TGF-β3 as control. (B) Optical density readings of TGF-β1. (C) Optical density readings of TGF-β3. (D) Concentrations were calculated based on optical density and reconfirmed following GF uptake readings from medias with known GF concentrations. Significant binding over baseline (binding to BSA, value of 0.1, grey box in B) indicated (n = 6, means ± SD). **P* = 0.001; Student's *t* test.

3F) as compared to the more dispersed HACs micromass samples (Figure 3A and 3E) after 28 days. The slight rise in the total number of necrotic cells in the centre of SSCs micromass samples is likely due, in part, to the larger size of the compact cell masses due to cell proliferation (7 and 5.1 times larger cluster area, normalised against area of cell clusters, in control sample for TGF-β1 and TGF-β3, respectively. Figure 3G). Hence, hypoxia may have been induced with cells at the centre of the compact mass potentially deprived of nutrients/oxygen. These observations are significant given current literature has evidenced viability but limited cell proliferation.[21]

3.3 Quantification of TGF-β in chondrobags

Fibronectin (FN) is known to have specific interactions with a diverse range of GFs, such as PDGF, FGF, IGF, TGF-β and others.[30, 50] The extent of this interaction varies within members of each superfamily. Within the TGF-β superfamily, TGF-β1, BMP-2, and BMP-7 display a high measure of affinity to a domain containing the 12th to 14th type III copies of FN (FN III12–14). However, in comparison, TGF-β2, TGF-β3, BMP-4, and BMP-6 did not exhibit notable binding to FN.[30] Consistent with this finding, GF release studies in chondrobags demonstrated that alginate-FN microgels display a 4-fold higher affinity for TGF-β1 in comparison to TGF-β3 (Figure 4). TGF-β1 was loaded and observed to be slowly released over 24 hours in alginate-FN hydrogels. In contrast, there was negligible release (and subsequent uptake) of TGF-β1 in alginate-based chondrobags, in the absence of FN. The same conditions examined for TGF-β3 in FN-free chondrobags resulted in no detectable readings (Figure 4). TGF-β1 and TGF-β3 interactions with FN result in modulation of their parting from the alginate-FN microgel (solid phase) to the soluble phase, hence regulating their diffusion, and dissipation concentration locally and consequently influencing cell signalling. We showed that higher local concentrations of TGF-β1 in chondrobags are influenced by the presence of FN. We hypothesise that TGF-β1 is bound to FN (FNIII12–14) and, given this occurs adjacent to the integrin binding region (FNIII9-10), provides the alginate-FN microgels with synergistic TGF-β1/integrin signalling leading into a highly permissive chondrogenic microenvironment [51] (Figure 2F).

3.4 Quantification of gene expression in HACs and SSCs cultured chondrobags

qPCR of chondrocyte-related marker transcripts was used to demonstrate the chondrogenic differentiation of SSCs (Figure 5K-T) and the phenotype maintenance of HACs (Figure 5A-J), following encapsulation within engineered alginate-FN chondrobags, with growth factors bound to FN and presented from a solid phase. The chondrogenic gene SOX9 has been observed during the in vitro induction of chondrogenesis and the subsequent promotion of the transcription of cartilage proteins, including type II collagen and aggrecan.[52] Type II collagen (COL2A1) is the predominant collagen present in physiological hyaline cartilage, providing cartilage with tensile strength.[53] Aggrecan (ACAN), the characteristic proteoglycan produced by chondrocytes, has been shown to link to collagen fibrils via hyaluronic acid. Importantly, the polyanionic nature of aggrecan draws water, which provides for cartilage expansion, key to the generation of mechanical function.[54]

Expression of *SOX9* (early marker), *COL2A1* (mid/late marker) and *ACAN* confirmed the potential of alginate-FN chondrobags to maintain the chondrogenic phenotype of HACs. These markers showed no significant differences between chondrobags loaded with either GFs; despite TGF-β3

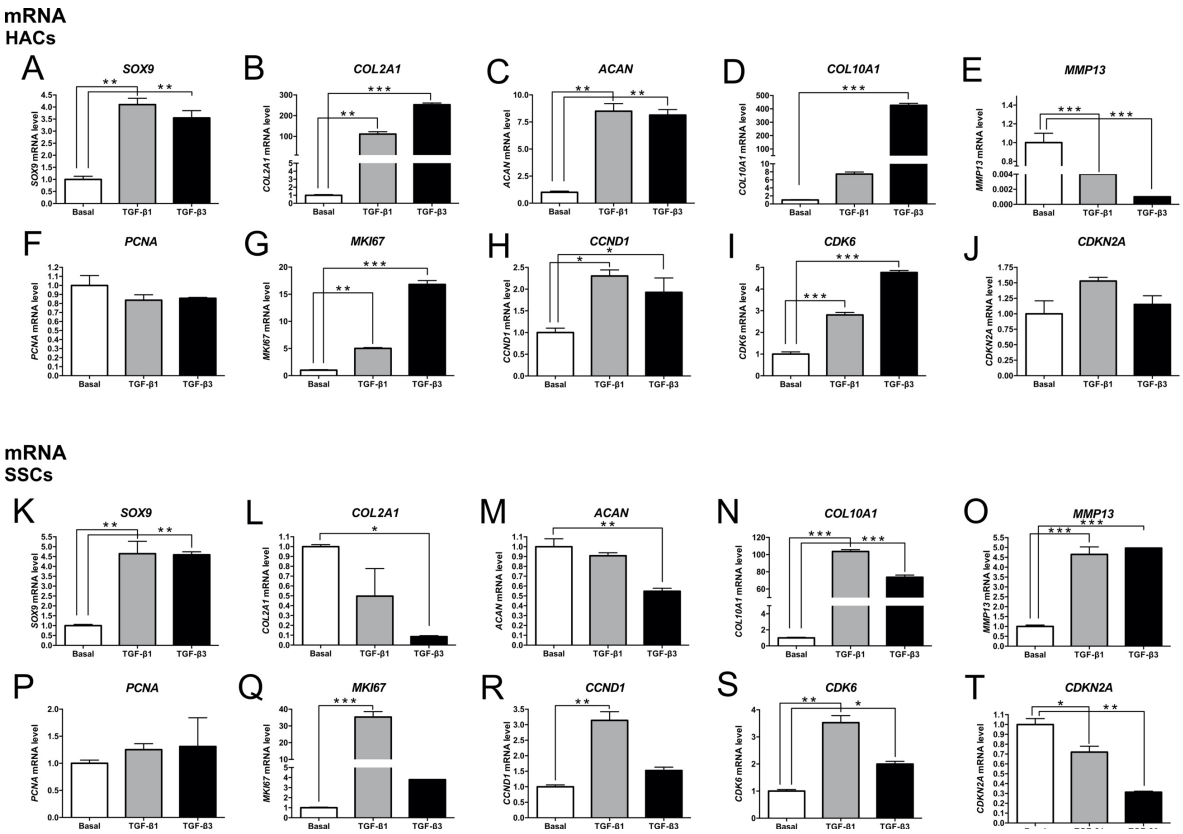

Figure 5. Gene expression in HACs and SSCs cultured within chondrobags. Chondrogenic, hypertrophic, proliferation and cell cycle specific gene expression in primary human articular chondrocytes (HACs) (A-J) and primary human skeletal stem cells (SSCs) (K-T) cultured in the presence of TGF-β1 or TGF-β3 for up to 28 days relative to untreated control. Differential expression of A-K: *SOX9*, B-L: *COL2A1*, C-M: *ACAN*, D-N: *COL10A1*, E-O: *MMP13*, F-P: *PCNA*, G-Q: *MKI67*, H-R: *CCDN1*, I-S: *CDK6*, J-T: *CDKN2A* analysed by qPCR. Values is the mean ± SD of triplicate determinations per sample. *p < 0.05, **p < 0.01, ***p < 0.001, one-way ANOVA.

not being bound to chondrobags with as high affinity as TGF-β1 (Figure 4). Chondrogenic associated SOX9 expression was observed to be notably up-regulated in HACs loaded with TGF-β1 (4.1-fold change) and loaded with TGF-β3 (3.6-fold change) (Figure 5A). This was also observed for COL2A1: with TGF-β1 (111.4-fold change) and treated with TGF-β3 (252.7-fold change) (Figure 5B), and ACAN: 8.5-fold change with TGF-β1 and 8.1-fold change treated with TGF-β3 (Figure 5C). This cumulative increase in the expression of COL2A1 and ACAN was in line with previous studies.[22, 55]

In contrast, SSCs did not display a clear and significant differentiation along the chondrogenic lineage. However, several studies have identified a discrete decrease in aggrecan expression for cells cultured within a 3D construct, supporting the current findings using SSCs (Figure 5M). Only SOX9 expression was significantly up-regulated following SSCs treatment with TGF-β1 (4.7-fold change) and treatment with TGF-β3 (4.6-fold change) (Figure 5K).

There are a number of markers of hypertrophic chondrocytes, with collagen type X and MMP13 the most widely recognised.[52, 56] Type X collagen functions as a substructure for ensuing matrix calcification.[57] Hypertrophic ECM functionally differs to physiological hyaline cartilage and, is in part, comparable to bone matrix. In this context, the current studies indicate that following 28 days of chondrogenic differentiation, HACs in chondrobags with TGF-β1 bound to FN displayed reduced commitment to the formation of hypertrophic chondrocytes, compared to cells stimulated with TGF-β3 (Figure 5D-E). Strikingly, the current results observed using engineered chondrobags, with TGF-β1 bound to FN, demonstrate negligible evidence of hypertrophic chondrocytes, enabling the maintenance of the required chondrocytic phenotype for cartilage tissue repair.

Specific genes for proliferation and cell cycle[58] were also examined. HACs and SSCs encapsulation in alginate-FN chondrobags resulted in modulation of essential components in G1/S, with decreased levels of p16 (*CDKN2A*), increased *CDK6* and cyclin expression (*CCDN1*), resulting in enhanced cell cycle progression and proliferation (Figure 5H-J and 5R-T). In the current study, we observed a significant up-regulation of *MKI67* in cells encapsulated in chondrobags with TGF-β1 bound to FN (5-fold change for HACs and 35-fold change for SSCs) (Figure 5G and 5Q) and to TGF-β3 (1.9-fold change for HACs and 1.5-fold change for SSCs) (Figure 5G and 5Q), indicating higher proliferative activity of cells within TGF-β3 alginate-FN chondrobags than cells within TGF-β1.

TGF-β1 appears to be closely connected with cell growth and differentiation providing a crucial role in the regulation of autocrine and paracrine processes.[59] In addition, TGF-β1 is a growth modulator with multi-physiological potencies on immune suppression and inflammation, cell differentiation,

wound healing and cancer.[60] However, Mueller and colleagues failed to detect any differences between aggregates preconditioned with TGF-β1 and TGF-β3 following histological evaluation and quantification of ALP secretion.[49] The likely differences from our study reside with the observation that in the engineered chondrobags, TGF-β1 is also bound to FN and presented from a solid phase (Figure 4), with TGF-β1 more accessible to the encapsulated cells and thus favouring chondrogenic differentiation.

3.5 microRNA profiling in HACs and SSCs cultured in chondrobags

Small noncoding RNAs (19-24 nucleotides long) have gained significant research interest in recent years.[61] MicroRNAs (miRNAs) in particular are important regulators of gene expression.[62] miRNAs are involved in the process of stem cell differentiation, together with stem cell therapy and can prompt skeletal regeneration and thus, miRNAs offer innovative approaches to prevent/treat OA and osteoporosis (OP)[63]. Following culture of HACs and SSCs with or without TGF- β1 or TGF- β3 for 28 days, TaqMan qPCR was used to determine the expression levels of miRNAs. miR-140 was employed as a positive control for chondrogenic differentiation.[64] Chondrogenic related miR-140-3p expression was notably up-regulated in the encapsulated cells in TGF-β1 alginate-FN chondrobags (61.8-fold change for HACs and 1.7-fold change for SSCs) (Figure 6A and 6D) and TGF-β3 alginate-FN chondrobags (81.2-fold change for HACs and 3.4-fold change for SSCs) (Figure 6A and 6D). miR-140 is an important modulator of cartilage homeostasis and implicated in OA. Critically, miR-140 is almost uniquely and abundantly expressed in chondrocytes[65] and, in addition, plays an important role in bone development, at least in part by controlling proliferation. Miyaki and collaborators reported that throughout chondrogenesis, miR-140 expression levels increase in differentiated human MSCs in comparison to undifferentiated MSC populations together with expression of *COL2A1*, *ACAN* and *SOX9*. These finding indicate miR-140 is a marker and potential modulator of chondrogenesis.[66]

In contrast, miR-146b expression was significantly down-regulated in cells encapsulated in TGF-β1 alginate-FN chondrobags (0.8-fold change for HACs and 0.1-fold change for SSCs) (Figure 6B and 6E) and in TGF-β3 alginate-FN chondrobags (0.5-fold change for HACs and 0.2-fold change for SSCs) (Figure 6B and 6E). Compared to chondrobags cultured in basal media, miR-146b was down-regulated during chondrogenic differentiation of human bone marrow derived SSCs. Furthermore, we have previously shown that miR-146b serves as a negative modulator of chondrogenesis, with an important role in the regulation of SOX5 expression during the chondrogenic differentiation of human bone marrow derived SSCs.[67]

miR-138 expression was observed to be notably up-regulated in HACs encapsulated in TGF-β3 alginate-FN chondrobags (1.4-fold change) but not with TGF-β1 (0.95-fold change) (Figure 6C). miR-138 expression in SSCs was significantly up-regulated under both conditions: 3.3-fold

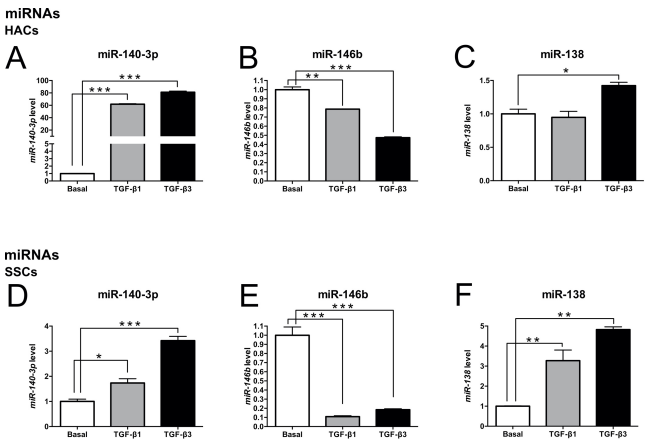

change with TGF-β1 and 4.8-fold change with TGF-β3 (Figure 6F). These results demonstrate the commitment of HACs and SSCs following culture for 28 days in the chondrobags towards the chondrogenic lineage. The overexpression of miR-138 has been shown to inhibit osteoblast differentiation hMSCs *in vitro.* miR-138 inhibition serves as an antimiR-138 for promoting expression of osteoblast-specific genes as well as the activity of alkaline phosphatase (ALP) and matrix mineralization.[68]

Figure 6. microRNA profiling in HACs and SSCs cultured within chondrobags. miRNA expression in primary human articular chondrocytes (HACs) (A-C) and primary human skeletal stem cells (SSCs) (D-F) cultured in the presence of TGF-β1 or TGF-β3 for up to 28 days relative to untreated control. Differential expression of A-D: miR-140, B-E: miR-146b, C-F: miR-138, analysed by TaqMan q-PCR. Values represent mean ± SD of duplicate determinations per sample. *$p < 0.05$, **$p < 0.01$, ***$p < 0.001$, one-way ANOVA.

3.6 Histological analysis of collagen formation in chondrobags

Chondrobags encapsulating HACs cultured *in vitro* for 28 days in the presence of TGF-β1 or TGF-β3 indicated enhanced cell proliferation evidenced by increased collagen deposits with faint Sirius Red staining compared to control (Figure 7). This result correlated with the observation of growth and proliferation observed in Figure 3 as well as gene expression results for proliferation and cell cycle markers in Figure 5F-J. In contrast, intense Alcian Blue stating (but not Sirius Red staining) was observed in the matrix of chondrobags cultured in the presence of TGF-β3 (Figure 7C) as compared to TGF-β1 (Figure 7B) indicating the formation of ECM (arrow). The comparatively intensive Alcian Blue staining of cartilage matrix and proteoglycans in chondrobags cultured in presence of TGF-β3 correlated with the observed gene expression studies of collagen II (*COL2A1*, Figure 5B) and collagen X (*COL10A1*, Figure 5D) from similarly treated samples. Safranin-O stains polyanions in alginate, [69] thus, the formation of new cartilage in the chondrobags can be difficult to determine. Nevertheless, the distribution of nuclei within the chondrobags can be clearly observed (Figure 7). The lack of fast green staining observed confirmed the absence of bone formation within these sections.

4. Conclusion

Notes

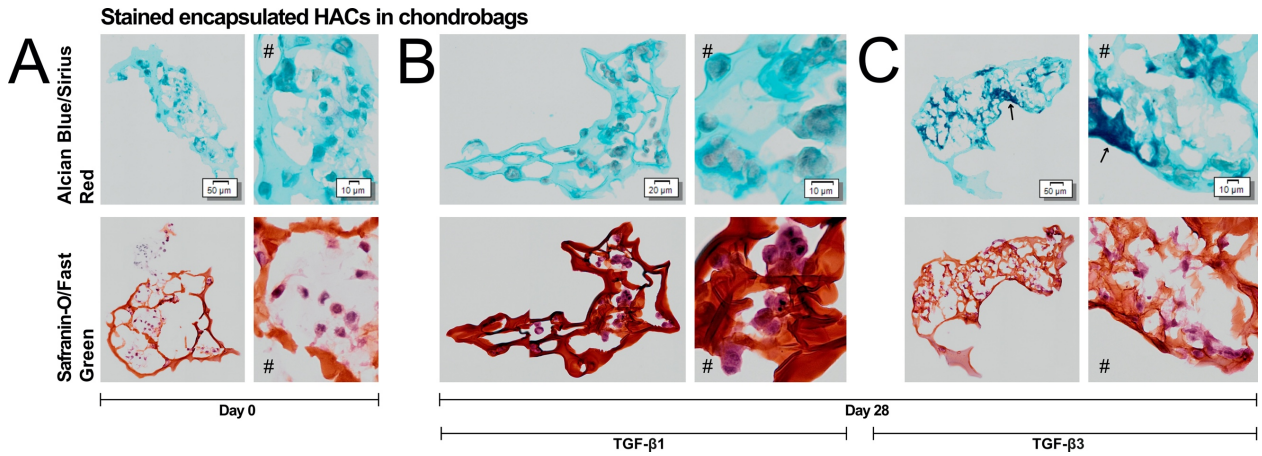

Figure 7. Stained encapsulated human articular chondrocytes (HACs) in alginate-fibronectin chondrobags. Alcian Blue/Sirius Red (top row) and Safranin O/Fast Green-stained (bottom row) histological sections of chondrocytes-laden chondrobags (5 µm sections). Histological appearance of chondrobags following basal culture for day 0 (A) and day 28 cultured in the presence of TGF-β1 (B) and day 28 cultured in the presence of TGF-β3 (C). All images accompanied with larger magnification (right images, #). Arrows are pointing to darker Alcian Blue staining as compared to the background lighter blue stain.

The current findings demonstrate that engineered TGF-β1 alginate-FN chondrobags provide an appropriate biomimetic environment for the formation of hyaline cartilage *in vitro*. We demonstrate that TGF-β1 bound to FN and presented from a solid phase, facilitates and enhances chondrogenic differentiation. Importantly, TGF-β1 loaded chondrobags promote chondrogenesis without the formation of hypertrophic chondrocytes. This cue-integrated-3D biomaterial platform, demonstrated increased proliferation, enhanced cell viability, chondrogenic differentiation of SSCs *in situ* and phenotype maintenance for HACs. The current studies illustrate the potential applications for a TGF-β1 alginate-FN chondrobags platform as a workable 3D bioprinting and culture system for cartilage tissue regeneration with therapeutic applications therein.

Acknowledgements

The support from the UK Engineering and Physical Sciences Research Council (EP/P001114/1) is acknowledged as well as support from the UK Regenerative Medicine Platform Hub Acellular SMART materials 3D architecture (MR/R015651/1) and a grant from the UK Regenerative Medicine Platform (MR/L012626/1 Southampton Imaging) is gratefully acknowledged. We thank Jon Ward and Carol Ann Smith for technical support.

Author Contributions

The manuscript was written through contributions from all authors. All authors have given approval to the final version of the manuscript. The authors, Kimia Witte and María C. de Andrés contributed equally.

The authors declare no competing financial interest.

All the original data related to this article are within the depository of the University of Glasgow (http://dx.doi.org/10.5525/gla.researchdata.871).

References

1. L. Moradi, M. Vasei, M. M. Dehghan, M. Majidi, S. Farzad Mohajeri, S. Bonakdar, *Biomaterials*, 2017, **126**, 18.
2. L. Kock, C. C. van Donkelaar, K. Ito, *Cell Tissue Res*, 2012, **347**, 613.
3. D. J. Hunter, D. T. Felson, *BMJ*, 2006, **332**, 639.
4. I. A. Otto, R. Levato, W. R. Webb, I. M. Khan, C. C. Breugem, J. Malda, *Eur Cell Mater*, 2018, **35**, 132.
5. G. Schulze-Tanzil, P. de Souza, H. Villegas Castrejon, T. John, H. J. Merker, A. Scheid, et al., *Cell Tissue Res*, 2002, **308**, 371.
6. A. M. Freyria, Y. Yang, H. Chajra, C. F. Rousseau, M. C. Ronziere, D. Herbage, et al., *Tissue Eng*, 2005, **11**, 674.
7. J. M. Jukes, L. Moroni, C. A. van Blitterswijk, J. de Boer, *Tissue Eng Part A*, 2008, **14**, 135.
8. M. Centola, B. Tonnarelli, S. Scharen, N. Glaser, A. Barbero, I. Martin, *Stem Cells Dev*, 2013, **22**, 2849.
9. P. Occhetta, M. Centola, B. Tonnarelli, A. Redaelli, I. Martin, M. Rasponi, *Sci Rep*, 2015, **5**, 10288.
10. B. K. Babur, K. Futrega, W. B. Lott, T. J. Klein, J. Cooper-White, M. R. Doran, *Cell Tissue Res*, 2015, **361**, 755.
11. F. Li, C. Levinson, V. X. Truong, L. A. Laurent-Applegate, K. Maniura-Weber, H. Thissen, et al., *Biomater Sci*, 2020, **8**, 1711.
12. M. Nie, S. Takeuchi, *Biofabrication*, 2018, **10**, 044103.

13. W. Swieszkowski, M. R. Dokmeci, A. Khademhosseini, *Biofabrication*, 2020, **12**, 030201.
14. R. S. Tare, J. C. Babister, J. Kanczler, R. O. Oreffo, *Mol Cell Endocrinol*, 2008, **288**, 11.
15. A. M. Freyria, M. C. Ronziere, D. Cortial, L. Galois, D. Hartmann, D. Herbage, et al., *Tissue Eng Part A*, 2009, **15**, 1233.
16. N. S. Hwang, S. Varghese, Z. Zhang, J. Elisseeff, *Tissue Eng*, 2006, **12**, 2695.
17. N. S. Hwang, S. Varghese, J. Elisseeff, *Methods Mol Biol*, 2007, **407**, 351.
18. G. Luca, M. Calvitti, C. Nastruzzi, L. Bilancetti, E. Becchetti, G. Angeletti, et al., *Tissue Eng*, 2007, **13**, 641.
19. H. L. Ma, S. C. Hung, S. Y. Lin, Y. L. Chen, W. H. Lo, *J Biomed Mater Res A*, 2003, **64**, 273.
20. J. Tritz-Schiavi, N. Charif, C. Henrionnet, N. de Isla, D. Bensoussan, J. Magdalou, et al., *Biomed Mater Eng*, 2010, **20**, 167.
21. J. C. Babister, R. S. Tare, D. W. Green, S. Inglis, S. Mann, R. O. Oreffo, *Biomaterials*, 2008, **29**, 58.
22. M. H. Park, R. Subbiah, M. J. Kwon, W. J. Kim, S. H. Kim, K. Park, et al., *Carbohydr Polym*, 2018, **202**, 488.
23. S. Degala, W. R. Zipfel, L. J. Bonassar, *Arch Biochem Biophys*, 2011, **505**, 112.
24. R. L. Mauck, B. A. Byers, X. Yuan, R. S. Tuan, *Biomech Model Mechanobiol*, 2007, **6**, 113.
25. C. N. Salinas, K. S. Anseth, *Biomaterials*, 2008, **29**, 2370.
26. S. Tavella, G. Bellese, P. Castagnola, I. Martin, D. Piccini, R. Doliana, et al., *J Cell Sci*, 1997, **110 (Pt 18)**, 2261.
27. J. Sottile, D. C. Hocking, *Mol Biol Cell*, 2002, **13**, 3546.
28. A. M. DeLise, L. Fischer, R. S. Tuan, *Osteoarthritis Cartilage*, 2000, **8**, 309.
29. P. A. Puolakkainen, J. E. Ranchalis, W. R. Gombotz, A. S. Hoffman, R. J. Mumper, D. R. Twardzik, *Gastroenterology*, 1994, **107**, 1319.
30. M. M. Martino, J. A. Hubbell, *FASEB J*, 2010, **24**, 4711.
31. L. A. Poniatowski, P. Wojdasiewicz, R. Gasik, D. Szukiewicz, *Mediators Inflamm*, 2015, **2015**, 137823.
32. C. G. Williams, T. K. Kim, A. Taboas, A. Malik, P. Manson, J. Elisseeff, *Tissue Eng*, 2003, **9**, 679.
33. F. Barry, R. E. Boynton, B. Liu, J. M. Murphy, *Exp Cell Res*, 2001, **268**, 189.
34. K. Witte, A. Rodrigo-Navarro, M. Salmeron-Sanchez, *Materials Today Bio*, 2019, **2**, 100011.
35. J. Kanczler, R. S. Tare, P. Stumpf, T. J. Noble, C. Black, R. O. C. Oreffo, *Methods Mol Biol*, 2019, **1914**, 53.
36. T. Andersen, P. Auk-Emblem, M. Dornish, *Microarrays (Basel)*, 2015, **4**, 133.
37. S. Sart, J. Bejoy, Y. Li, *Process Biochemistry*, 2017, **59**, 276.
38. S. Cascone, G. Lamberti, *International Journal of Pharmaceutics*, 2020, **573**, 118803.
39. C. Shao, J. Chi, H. Zhang, Q. Fan, Y. Zhao, F. Ye, *Advanced Materials Technologies*, 2020, 2000183.
40. E. L. Jackson-Holmes, T. C. McDevitt, H. Lu, *Lab on a Chip*, 2017, **17**, 3634.
41. I. Paik, D. J. Scurr, B. Morris, G. Hall, C. Denning, M. R. Alexander, et al., *Biotechnol Bioeng*, 2012, **109**, 2630.
42. R. Yoshimitsu, K. Hattori, S. Sugiura, Y. Kondo, R. Yamada, S. Tachikawa, et al., *Biotechnology and Bioengineering*, 2014, **111**, 937.
43. C. Gaut, K. Sugaya, *Regen Med*, 2015, **10**, 665.
44. T. D. Bornes, N. M. Jomha, A. Mulet-Sierra, A. B. Adesida, *Stem Cell Res Ther*, 2015, **6**, 84.
45. M. Sarem, M. Heizmann, A. Barbero, I. Martin, V. P. Shastri, *Proc Natl Acad Sci U S A*, 2018, **115**, E6135.
46. C. J. Centeno, D. Busse, J. Kisiday, C. Keohan, M. Freeman, D. Karli, *Med Hypotheses*, 2008, **71**, 900.
47. V. Dexheimer, S. Frank, W. Richter, *Stem Cells Dev*, 2012, **21**, 2160.
48. R. T. Ballock, R. J. O'Keefe, *Birth Defects Res C Embryo Today*, 2003, **69**, 123.
49. M. B. Mueller, M. Fischer, J. Zellner, A. Berner, T. Dienstknecht, L. Prantl, et al., *Cells Tissues Organs*, 2010, **192**, 158.
50. M. Salmeron-Sanchez, M. J. Dalby, *Chem Commun (Camb)*, 2016, **52**, 13327.
51. M. M. Martino, F. Tortelli, M. Mochizuki, S. Traub, D. Ben-David, G. A. Kuhn, et al., *Sci Transl Med*, 2011, **3**, 100ra89.
52. D. Studer, C. Millan, E. Ozturk, K. Maniura-Weber, M. Zenobi-Wong, *Eur Cell Mater*, 2012, **24**, 118.
53. A. R. Poole, T. Kojima, T. Yasuda, F. Mwale, M. Kobayashi, S. Laverty, *Clin Orthop Relat Res*, 2001, S26.
54. C. C. Wang, K. C. Yang, K. H. Lin, Y. L. Liu, H. C. Liu, F. H. Lin, *Biomaterials*, 2012, **33**, 120.
55. P. Karunanithi, M. R. Murali, S. Samuel, H. R. B. Raghavendran, A. A. Abbas, T. Kamarul, *Carbohydr Polym*, 2016, **147**, 294.
56. P. M. van der Kraan, W. B. van den Berg, *Osteoarthritis Cartilage*, 2012, **20**, 223.
57. G. Shen, *Orthod Craniofac Res*, 2005, **8**, 11.
58. G. K. Schwartz, M. A. Shah, *J Clin Oncol*, 2005, **23**, 9408.
59. R. Govinden, K. D. Bhoola, *Pharmacol Ther*, 2003, **98**, 257.
60. M. B. Sporn, A. B. Roberts, L. M. Wakefield, R. K. Assoian, *Science*, 1986, **233**, 532.
61. V. S. Patil, R. Zhou, T. M. Rana, *Crit Rev Biochem Mol Biol*, 2014, **49**, 16.
62. X. Liu, K. Fortin, Z. Mourelatos, *Brain Pathol*, 2008, **18**, 113.

63. E. Budd, S. Waddell, M. C. de Andres, R. O. C. Oreffo, *Curr Mol Biol Rep*, 2017, **3**, 263.
64. T. A. Karlsen, R. B. Jakobsen, T. S. Mikkelsen, J. E. Brinchmann, *Stem Cells Dev*, 2014, **23**, 290.
65. L. Tuddenham, G. Wheeler, S. Ntounia-Fousara, J. Waters, M. K. Hajihosseini, I. Clark, et al., *FEBS Lett*, 2006, **580**, 4214.
66. S. Miyaki, T. Nakasa, S. Otsuki, S. P. Grogan, R. Higashiyama, A. Inoue, et al., *Arthritis Rheum*, 2009, **60**, 2723.
67. E. Budd, M. C. de Andres, T. Sanchez-Elsner, R. O. C. Oreffo, *Sci Rep*, 2017, **7**, 46704.
68. T. Eskildsen, H. Taipaleenmaki, J. Stenvang, B. M. Abdallah, N. Ditzel, A. Y. Nossent, et al., *Proc Natl Acad Sci U S A*, 2011, **108**, 6139.
69. A. Moshaverinia, X. Xu, C. Chen, K. Akiyama, M. L. Snead, S. Shi, *Acta Biomater*, 2013, **9**, 9343.